NG2 glia protect against prion neurotoxicity by inhibiting prostaglandin E2 signaling

Yingjun Liu[1, *], Jingjing Guo[1], Maja Matoga[1], Marina Korotkova[2], Per-Johan Jakobsson[2], Adriano Aguzzi[1, *]

[1] Institute of Neuropathology, University of Zurich, Switzerland

[2] Department of Medicine, Karolinska Institutet, Sweden

[*] Correspondence

Adriano Aguzzi or Yingjun Liu:

Institute of Neuropathology, University of Zurich,

Schmelzbergstrasse 12, 8091 Zurich, Switzerland.

Telephone: +41 44 255 21 07.

Email: adriano.aguzzi@usz.ch or yingjun.liu@bsse.ethz.ch

Abstract

Oligodendrocyte-lineage cells of patients and animal models undergo prominent changes in various neurodegenerative disorders. This raises the question of how myelinating cells interact with neurodegenerative processes. Here, we investigated the role of oligodendrocyte precursor cells (NG2 glia) in prion infections. We found that NG2 glia were activated in prion-infected cerebellar organotypic cultured slices (COCS) and in brains of prion-inoculated mice. In both model systems, depletion of NG2 glia exacerbated prion-induced neurodegeneration and accelerated prion pathology, suggesting a protective effect for NG2 glia. Loss of NG2 glia unleashed a microglial reaction promoting the biosynthesis of prostaglandin E2 (PGE2), which augmented prion toxicity in HovS cells and COCS through binding to the EP1 and EP4 receptors. Pharmacological or genetic inhibition of PGE2 biosynthesis attenuated prion-induced neurodegeneration in COCS and mice, antagonized the enhanced neurodegeneration in NG2 glia-depleted COCS and brains after prion infection, and dampened the acceleration of prion disease in NG2 glia-depleted mice. These data unveil a non-cell-autonomous interaction involving NG2 glia and microglia in prion disease and suggest that PGE2 signaling may represent an actionable target against prion diseases.

Introduction

Neurodegenerative diseases such as Alzheimer's disease (AD), Parkinson's disease (PD) and prion diseases involve multiple cell types and various genetic and environmental factors (Wareham, Liddelow et al. 2022). Accumulating evidence suggest that both cell-autonomous and non-cell-autonomous mechanisms contribute to the neurodegenerative process (Liu and Aguzzi 2019). Among the common neurodegenerative disorders, prion disease can be best mimicked with laboratory animal models (Aguzzi and Liu 2017). Prion-inoculated mice develop a fatal neurodegenerative condition that is almost indistinguishable from its human counterpart at the neuropathological level, providing an invaluable model system for investigating the cellular and molecular mechanisms of chronic neurodegeneration relevant to humans.

Different neurodegenerative diseases have distinct initial pathogenic triggers and clinical manifestations, yet certain molecular and cellular alterations, such as abnormal protein aggregation and activation of glial cells, are common to all these disorders (Wareham, Liddelow et al. 2022). Large amounts of data support vital roles of microglia and astrocytes in the initiation and progression of neurodegeneration. However, the function of other cell types, including oligodendrocyte-lineage cells, in the pathogenesis of neurodegenerative diseases has been elusive, and investigations on this crucial aspect were largely ignored by the neurodegenerative disease community. Recent advances in high resolution gene expression analyses have enabled a deeper understanding of this complex cellular landscape. In addition to confirming the alterations of microglia and astrocytes, single-cell and spatial transcriptomics analyses of brain tissues from patients and animal models have unraveled prominent changes of oligodendrocyte linage cells in multiple neurodegenerative disorders (Mathys, Davila-Velderrain et al. 2019, Chen, Lu et al. 2020, Pandey, Shen et al. 2022), including prion disease (Dimitriadis, Zhang et al. 2022, Slota, Sajesh et al. 2022).

Oligodendrocyte-lineage cells are traditionally considered as supportive cells in the central nervous system (CNS), producing myelin sheaths that insulate nerve fibers and help speed up transmission of electrical signals along neuronal axons. It is unclear how myelinating cells interact with other cell types of the brain in the context of neurodegenerative process. Here we investigated the role of oligodendrocyte precursor cells (NG2 glia) in chronic neurodegeneration induced by prion infections. We found that NG2 glia were neuroprotective and played a crucial role in controlling microglial pathway that is responsible for the biosynthesis of prostaglandin E2 (PGE2), which promotes prion-induced neurodegeneration through binding to the EP1 and EP4 receptors. These data place NG2 glia at the center of an intricate cell-cell interaction network in prion disease, and highlight NG2 glia and PGE2 signaling as potential targets for disease-modifying therapies against neurodegenerative disorders.

Results

NG2 glia activation in prion disease models

Our previous gene expression analyses of prion-inoculated mice (Sorce, Nuvolone et al. 2020) and prion-infected cerebellar organotypic cultured slices (COCS) (Liu, Senatore et al. 2022), as well as recent single-cell transcriptomics from other groups (Dimitriadis, Zhang et al. 2022, Slota, Sajesh et al. 2022), point to possible transcriptional changes in NG2 glia during prion infections. However, it is unclear how these cells respond to prion infection at the cellular level. We therefore examined the markers of NG2 glia, including NG2 and platelet-derived growth factor receptor alpha (Pdgfrα), in prion-infected COCS and mouse brains by western blotting and immunofluorescence. We found a strong increase in NG2 protein levels in both paradigms

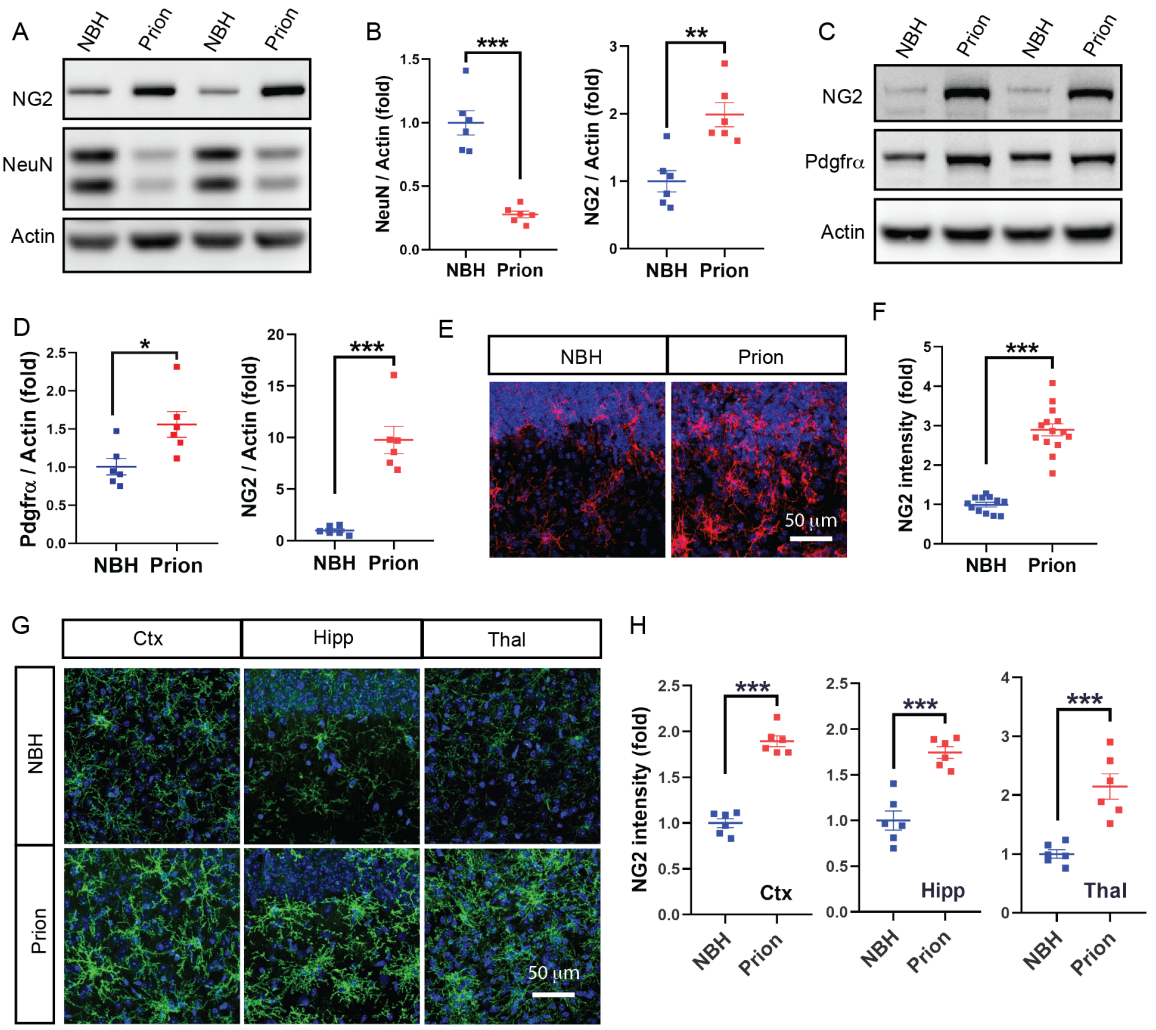

Figure 1, NG2 glia activation in prion disease models. **A-B**, Western blots (A) and quantification (B) of NG2 and NeuN in COCS exposed to prions or non-infectious brain homogenates (NBH, here and in all subsequent figures). n = 6 samples/condition; 6-8 slices/sample. **C-D**, Western blots (C) and quantification (D) of NG2 and Pdgfrα in brain tissues of mice infected with prions or inoculated with NBH. n = 6 mice/condition. **E**, NG2 immunofluorescent images showing NG2 glia activation in prion-infected COCS vs COCS exposed to NBH. Nuclei were stained with DAPI (blue), here and henceforth. **F**, Quantifications of NG2 immuno-intensity shown in E. n = 12 slices for NBH; n = 14 slices for Prion. **G**, NG2 glia activation in the cerebral cortex (Ctx), hippocampus (Hip) and thalamus (Thal) of prion-inoculated mice vs mice inoculated with NBH. **H**, Quantifications of NG2 immuno-intensity shown in G. n = 6 mice/group. Here and in all following figures: *: $p < 0.05$; **: $p < 0.01$; ***: $p < 0.001$; n.s: not significant.

(**Fig. 1A-D**) after prion infection. The protein level of Pdgfrα was also upregulated in prion-inoculated mouse brains, although not as much as NG2 (**Fig. 1C-D**). Similarly, we observed enhanced NG2 immunoreactivity in prion-infected COCS and prion-inoculated mouse brains (**Fig. 1E-H**). After prion infection, NG2 glia exhibited conspicuous enlargement of cell bodies and extensive arborization of cellular processes (**Fig. 1G**), reminiscent of the NG2 glia activation phenotype in mouse models of brain injuries (Alonso 2005, Jin, Riew et al. 2018).

Loss of NG2 glia enhances prion-induced neurodegeneration and accelerates prion disease

To facilitate functional investigations of NG2 glia, we previously developed efficient and selective NG2 glia depletion strategies ex vivo and in vivo (Liu and Aguzzi 2020). We used the PDGFR inhibitor CP673451 to deplete NG2 glia from COCS, and combined cell-type specific diphtheria toxin receptor (DTR) expression with short-term systemic DT injections for in vivo NG2 glia depletion.

To determine the functional relevance of NG2 glia in prion-induced neurodegeneration, we depleted NG2 glia from COCS by continuous (**Supplementary fig. 1A**) or transient (**Supplementary fig. 1B**) CP673451 treatment in the presence or absence of prions, and compared them to DMSO treated controls. Again, we saw enhanced NG2 immunoreactivity in prion-infected COCS and – as expected – robust NG2 glia loss in both uninfected and prion-infected COCS after continuous CP673451 treatment (**Fig. 2A-B**). Although NG2 glia depletion did not influence neuronal survival in the absence of prions, it strongly enhanced neurodegeneration in prion exposed COCS (**Fig. 2A-B**), suggesting a neuroprotective role of NG2 glia under pathological conditions. A similar enhancement of neurodegeneration was also observed in prion-infected COCS after transient CP673451 treatment (**Supplementary fig. 1C-D**). Interestingly, NG2 glia number was largely restored 3 weeks after transient CP673451 treatment in prion-infected COCS (**Supplementary fig. 1C-D**), suggesting that short-term destruction of NG2 glia suffices to influence prion neurotoxicity.

To investigate the effects of NG2 glia depletion on prion disease development in vivo, we crossed Pdgfrα-CreER mice with iDTR mice and generated Pdgfrα-CreER/iDTR (Pdgfrα^{iDTR}) mice. Pdgfrα-CreER and iDTR littermates were used for control. We inoculated mice with prions one month after tamoxifen treatment, and administered DT daily for 5 days at 12 or 16-weeks post inoculation (wpi) (**Supplementary fig. 2A**). According to immunofluorescent examinations, there was ~50% decrease of NG2 glia number in the brains of Pdgfrα^{iDTR} mice compared to controls after DT injection (Liu and Aguzzi 2020). Prion disease development was vastly accelerated in NG2 glia-depleted Pdgfrα^{iDTR} mice of both sexes when NG2 glia depletion was induced at 16 wpi (**Fig. 2C**) and in male mice when NG2 glia depletion was induced at 12 wpi (**Supplementary fig. 2B**), possibly attributable to the sex effects on the

incubation time of prion disease in animal models (Loeuillet, Boelle et al. 2010, Akhtar, Wenborn et al. 2011).

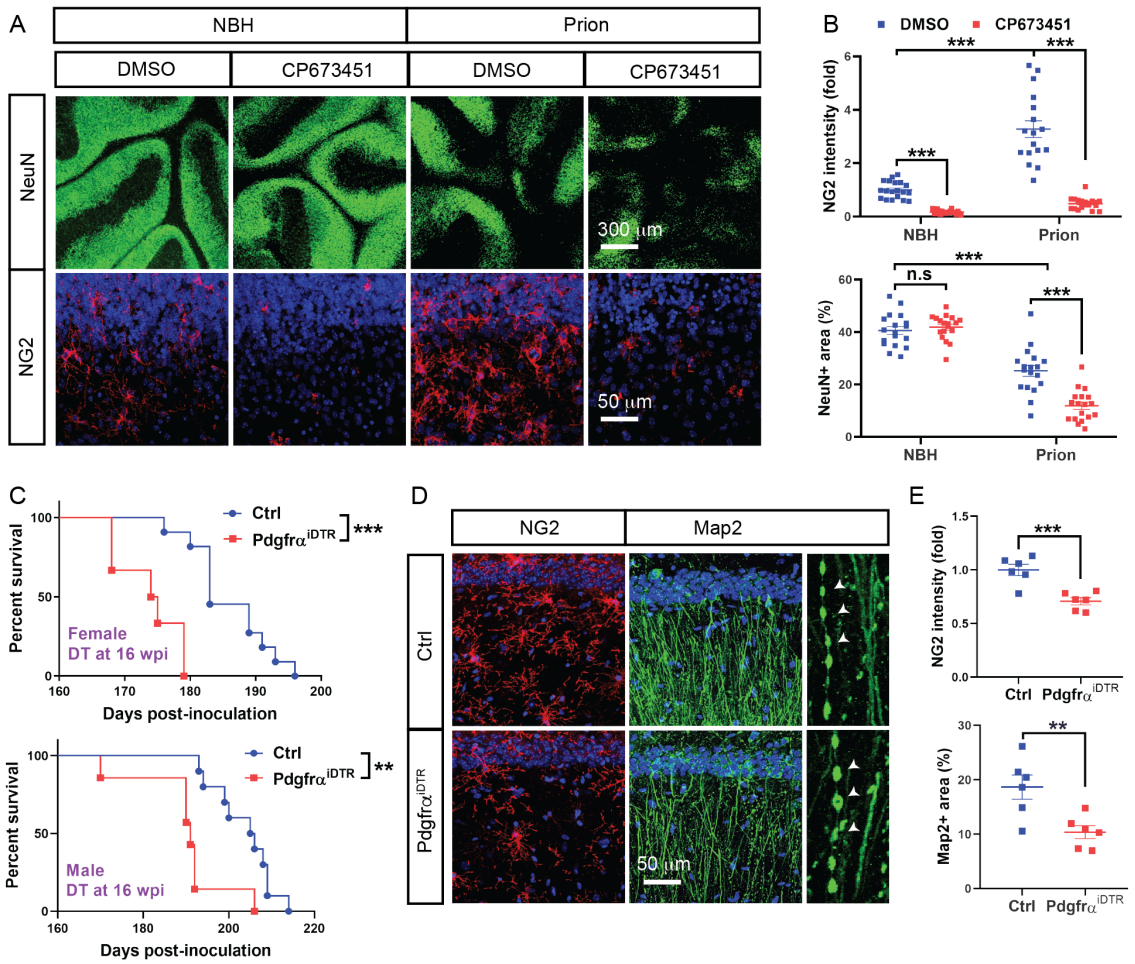

Figure 2, NG2 glia depletion enhances prion-induced neurodegeneration and accelerates disease development. **A**, NeuN and NG2 immunofluorescence showing neurodegeneration in prion-infected NG2 glia-depleted (CP673451) or intact (DMSO) COCS. **B**, Quantifications of NG2 immuno-intensity and NeuN positive area shown in A. n > 16 slices/condition. **C**, Survival curves showing accelerated prion disease in NG2 glia-depleted (Pdgfrα^{iDTR}) mice after prion inoculation. NG2 glia depletion was induced at 16 wpi. **D**, NG2 and Map2 immunofluorescence showing enhanced dendritic pathology in hippocampi of NG2 glia-depleted (Pdgfrα^{iDTR}) mice after prion inoculation. Arrowheads: pathologic dendrites with varicosities and fragmentation. NG2 glia depletion was induced at 16 wpi; brains were collected at 21 wpi. **E**, Quantifications of NG2 immuno-intensity and Map2 positive area shown in D. n = 6 mice/group.

Early neurodegeneration in prion disease is characterized by severe dendritic pathology (Fuhrmann, Mitteregger et al. 2007), which can be best visualized in the hippocampus. To investigate whether loss of NG2 glia affects prion-induced neurodegeneration in vivo, we inoculated a second cohort of Pdgfrα^{iDTR} and control mice after tamoxifen treatment, administered DT at 16 wpi and collected brains 4 weeks thereafter at ~21 wpi. Immunostaining of NG2 confirmed reduction of NG2 glia number in Pdgfrα^{iDTR} mice compared to controls (**Fig. 2D-E**). We then examined hippocampal dendritic pathology by Map2 immunofluorescence. As expected, we observed dendritic damages characterized by dendritic varicosities and fragmentation in both NG2 glia intact and NG2 glia depleted mice after prion infection (**Fig. 2D**).

However, the density of surviving dendrites was much less in Pdgfrα^{iDTR} mice than in control mice (**Fig. 2D-E**), suggesting that NG2 glia deficiency also enhances prion-induced neurodegeneration in vivo.

Loss of NG2 glia does not influence PrP^{C} expression, prion replication and prion-induced neuroinflammation

PrP^{C} is the substrate of prion replication (Bueler, Aguzzi et al. 1993) and is essential for prion disease pathogenesis (Brandner, Isenmann et al. 1996). Tissue abundance of PrP^{C} correlates with the incubation time of prion disease in animal models (Fischer, Rulicke et al. 1996, Minikel, Zhao et al. 2020). We therefore examined the levels of PrP^{C} and PrP^{Sc} (the protease K-resistant pathological PrP) in NG2 glia-depleted COCS and mice by western blotting. We found that neither the PrP^{C} (**Supplementary fig. 3A-B**) nor the PrP^{Sc} levels (**Supplementary fig. 3C-D**) noticeably changed in COCS treated with CP673451 compared to DMSO-treated controls. Similar levels of PrP^{C} (**Supplementary fig. 3E-F**) and PrP^{Sc} (**Supplementary fig. 3G-H**) were observed in the brains of NG2 glia depleted Pdgfrα^{iDTR} mice and NG2 glia intact control mice. Hence, enhanced neurodegeneration and accelerated prion disease after NG2 glia depletion were not caused by alterations of PrP^{C} expression and prion replication.

We previously found that NG2 glia were required for maintaining the homeostatic microglia state (Liu and Aguzzi 2020). However, depletion of NG2 glia in cultured brain slices and adult mice did not influence microglia numbers or induce notable changes of neuroinflammatory responses under normal conditions (Liu and Aguzzi 2020). To determine whether loss of NG2 glia affects prion-induced microglia activation and neuroinflammation, we compared the density of Cd68^{+} reactive microglia between NG2 glia-depleted and intact COCS in the presence or absence of prions. Reactive microglia were rare in control COCS, but their number increased conspicuously after prion infection (**Supplementary fig. 4A-B**). Nevertheless, the levels of microglia activation were comparable between NG2 glia-depleted and intact COCS, with or without prion infections (**Supplementary fig. 4A-B**). Similarly, we did not observe any changes of Iba1 and Cd68 immunoreactivity in NG2 glia-depleted brains after prion infection (**Supplementary fig. 4C-D**). Furthermore, the mRNA levels of the proinflammatory factors, tumor necrosis factor alpha (TNFα), Interleukin 1 beta (IL1β) and IL12β, were unaltered by NG2 glia depletion in COCS and mouse brains after prion infection (**Supplementary fig. 5A-B**). Collectively, these data suggest that loss of NG2 glia does not modulate prion-induced microglia activation and neuroinflammation.

Loss of NG2 glia enhances pathway that is responsible for PGE2 biosynthesis

When evaluating gene expression changes in NG2 glia depleted COCS with RNA-seq and qRT-PCR (Liu and Aguzzi 2020), we noticed possible dysregulation of the biosynthesis of PGE2, which was reported to increase in the cerebral spinal fluid (CSF) of prion disease patients (Minghetti, Greco et al. 2000, Minghetti, Cardone et al. 2002).

To confirm the potential influence of NG2 glia on PGE2, we depleted NG2 glia in COCS with CP673451, and examined the expression levels of cyclooxygenase 2 (Cox2) and prostaglandin E synthase (Ptges), two major enzymes responsible for the biosynthesis of PGE2 under pathological conditions. Both immunofluorescence and qRT-PCR results confirmed efficient NG2 glia depletion after CP673451 treatment (**Fig. 3A-C**). Importantly, we found that the expression levels of both Cox2 and Ptges were strikingly upregulated in NG2 glia depleted

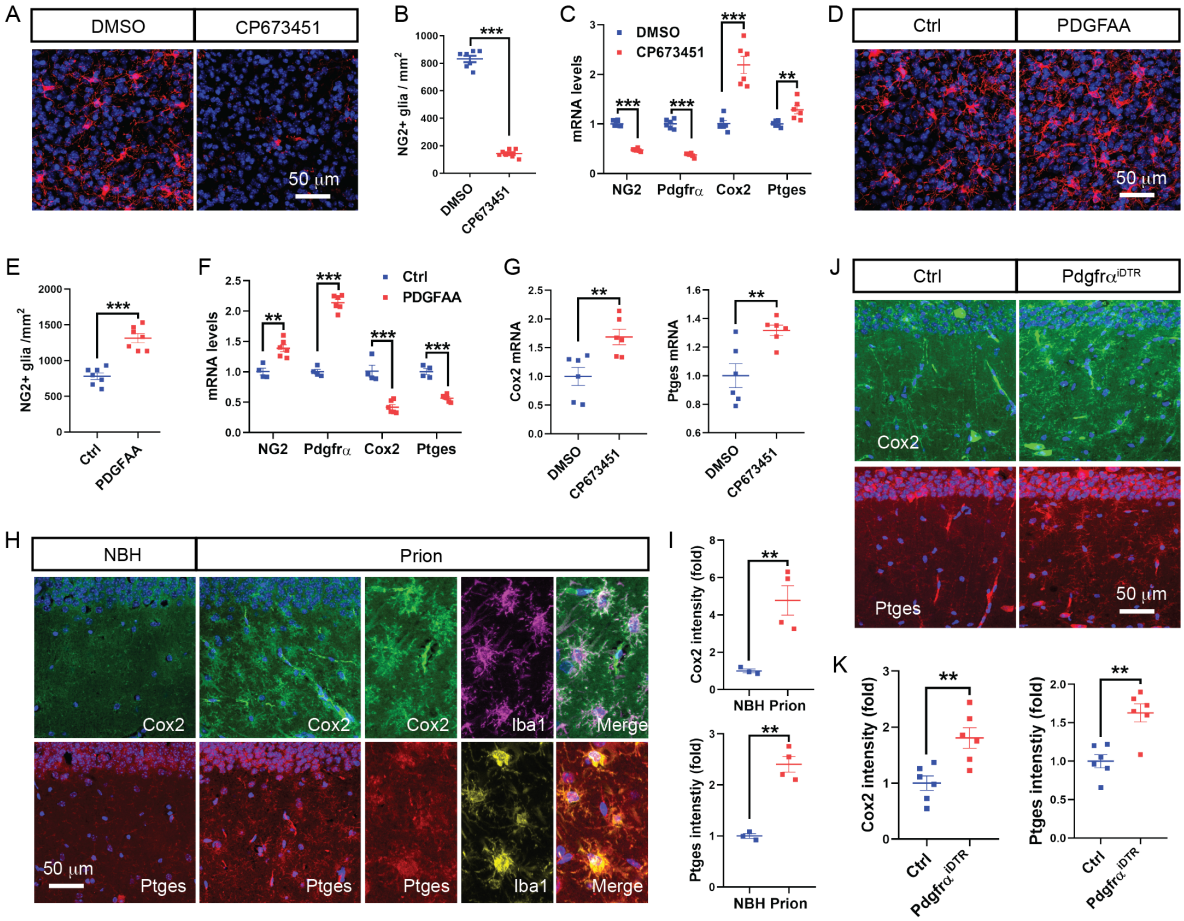

Figure 3, Loss of NG2 glia upregulates Cox2-Ptges expression. **A-B**, NG2 immunofluorescence (A) and quantification (B) in NG2 glia intact (DMSO) and depleted (CP673451) COCS. n = 7 slices/condition. **C**, qRT-PCR showing downregulation of NG2 and Pdgfrα and upregulation of Cox2 and Ptges in NG2 glia-depleted (CP673451) COCS. n = 6 samples; 6-8 slices/sample. **D-E**, NG2 immunofluorescence (D) and quantification (E) in intact (Ctrl) and PDGFAA-treated COCS. n = 7 slices/condition. **F**, qRT-PCR results showing upregulation of NG2 and Pdgfrα and downregulation of Cox2 and Ptges in COCS with increased NG2 glia density (PDGFAA) compared to NG2 glia intact (Ctrl) COCS. n = 6 samples; 6-8 slices/sample. **G**, qRT-PCR showing upregulation of Cox2 and Ptges in NG2 glia-depleted (CP673451) COCS after prion exposure. n = 6 samples; 6-8 slices/sample. **H**, Cox2, Ptges and Iba1 immunofluorescence showing upregulation of Cox2 and Ptges and their colocalization with microglia in brains of terminally sick prion-inoculated mice compared to NBH-inoculated mice. **I**, Quantifications of Cox2 and Ptges immuno-intensity shown in H. n = 3 mice for NBH and n = 4 mice for prion. **J**, Cox2 and Ptges immunofluorescence showing upregulation of Cox2 and Ptges in the brains of NG2 glia depleted (Pdgfrα^{iDTR}) mice compared to NG2 glia intact (Ctrl) mice after prion inoculation. **K**, Quantification of Cox2 and Ptges immuno-intensity shown in J. n = 6 mice/group.

COCS compared to NG2 glia intact COCS (**Fig. 3C**). Furthermore, we treated COCS with PDGFAA, the ligand for Pdgfrα, which promotes NG2 glia proliferation (Calver, Hall et al. 1998). Immunofluorescent and qRT-PCR results indicated notable increase of NG2 glia density in PDGFAA-treated COCS compared to controls (**Fig. 3D-F**). We found that increase of NG2 glia number drastically decreased the expression levels of both Cox2 and Ptges (**Fig. 3F**). These data indicate that NG2 glia tightly control the PGE2 biosynthesis pathway. In line with the above findings, drastic upregulation of both Cox2 and Ptges were also observed in NG2 glia-depleted COCS after prion infection (**Fig. 3G**). As comparison, neither Cox1 nor Ptgds significantly changed upon NG2 glia depletion (**Supplementary fig. 6**).

To investigate if loss of NG2 glia induces similar changes of Cox2 and Ptges in vivo, we examined the expression levels of Cox2 and Ptges and their cellular localization in the brain by immunofluorescence. We found that the immunoreactivity of both Cox2 and Ptges were relatively low under normal condition (**Fig. 3H-I**); however, prion infection drastically increased their expression levels (**Fig. 3H-I**), especially in microglia (**Fig. 3H**). NG2 glia depletion remarkably increased prion-induced upregulation of Cox2 and Ptges (**Fig. 3J-K**), suggesting that NG2 glia also control this pathway in vivo.

Inhibition of PGE2 biosynthesis diminishes prion-induced neurodegeneration and decelerates prion disease

Although previous studies indicated that the level of PGE2 in the CSF was increased in prion-diseased patients (Minghetti, Greco et al. 2000, Minghetti, Cardone et al. 2002) and was positively correlated with the progression rate of sporadic Creutzfeldt-Jakob disease (Minghetti, Greco et al. 2000), it is unclear whether PGE2 plays a causal role in prion-induced neurodegeneration. To investigate this, we treated normal and prion-infected COCS with PGE2 and PGD2, or DMSO as control, and examined neurodegeneration by NeuN immunofluorescence. PGE2 treatment had no effect on neuronal survival under normal conditions but drastically enhanced neuronal death in prion-infected COCS (**Fig. 4A-B**). In contrast, prion-induced neurodegeneration in PGD2 treated COCS was largely unaltered compared to DMSO (**Fig. 4A-B**). To investigate whether inhibition of PGE2 biosynthesis protects prion-induced neurodegeneration, we treated normal and prion-infected COCS with C118 or C934 (Larsson, Steinmetz et al. 2019), two highly selective Ptges inhibitors. Remarkably, both Ptges inhibitors strongly reduced neurodegeneration in prion-exposed COCS (**Fig. 4C-D**). These results suggest that PGE2 is a potent enhancer of prion neurotoxicity, and inhibition of PGE2 biosynthesis is neuroprotective.

To investigate the effects of PGE2 biosynthesis inhibition on prion disease in vivo, we inoculated Cox2Luc mice, in which the Cox2 gene was replaced with the coding sequence of luciferase, and control mice with prions. We found that Cox2Luc mice survived significantly longer

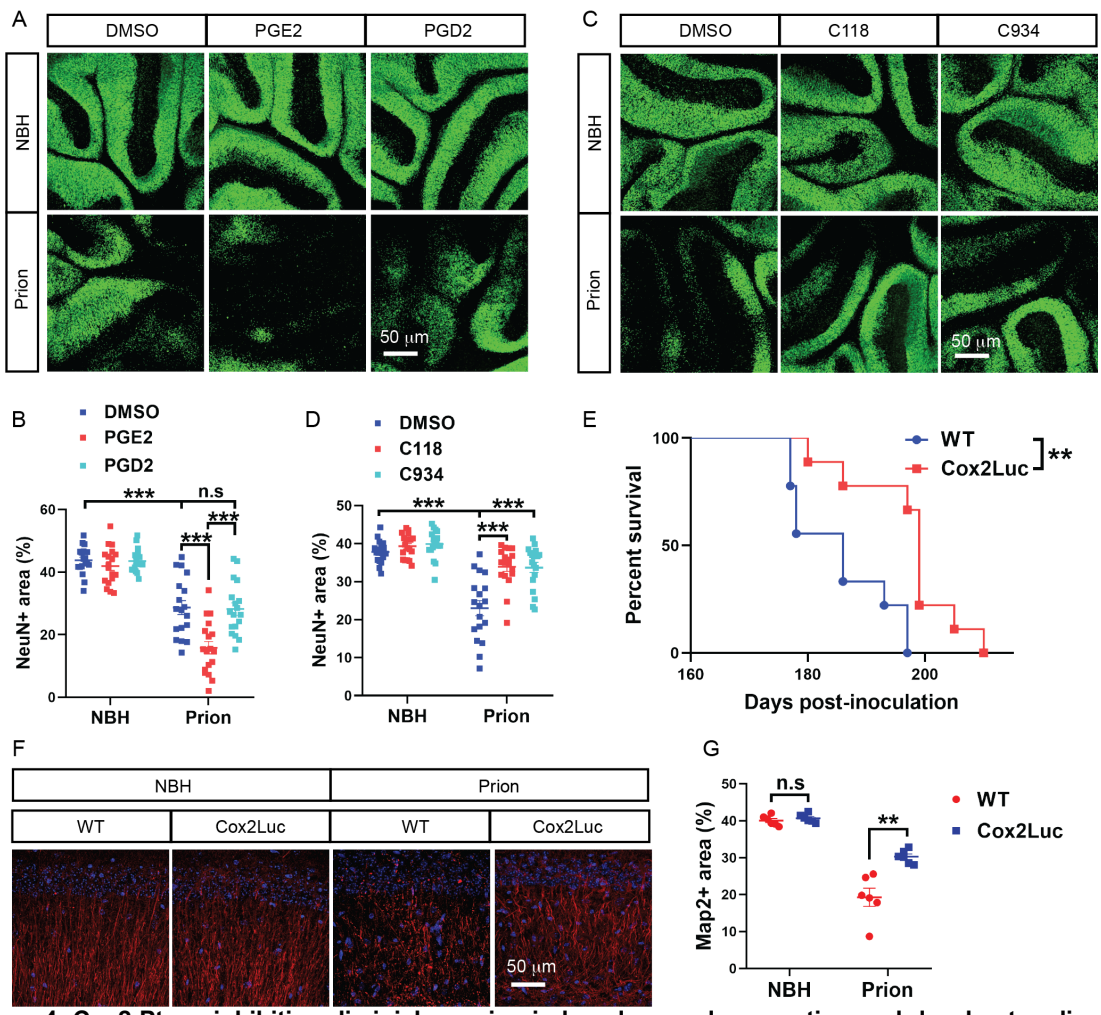

Figure 4, Cox2-Ptges inhibition diminishes prion-induced neurodegeneration and decelerates disease development. **A-B**, NeuN immunofluorescence (A) and quantification (B) showing enhanced neurodegeneration in PGE2 treated compared to DMSO treated and PGD2 treated COCS after prion infection. n = 18 slices/condition. **C-D**, NeuN immunofluorescence (C) and quantification (D) showing diminished neurodegeneration in COCS treated with Ptges inhibitors C118 and C934 compared to DMSO treated COCS after prion infection. n = 18 slices/condition. **E**, Survival curves showing decelerated prion disease in Cox2 knockout (Cox2Luc) mice compared to littermate WT mice. **F-G**, Map2 immunofluorescence (F) and quantification (G) showing diminished dendritic pathology in the hippocampi of Cox2Luc mice after prion inoculation compared to littermate WT mice. Brain samples were collected at 21 wpi. n = 6 mice/group.

than their littermate controls after prion infection (**Fig. 4E**), suggesting that elevation of Cox2 and PGE2 production during prion disease are detrimental in vivo. In consistent with this, immunofluorescent staining of Map2 demonstrated ameliorated prion-induced dendritic pathology in the hippocampus of the Cox2Luc mice compared to controls (**Fig. 4F-G).**

Inhibition of PGE2 biosynthesis rescues the enhanced neurodegeneration and accelerated prion disease after NG2 glia depletion

Next, we investigated whether the upregulation of Cox2 and Ptges and the subsequent increase of PGE2 biosynthesis were responsible for the enhanced prion neurotoxicity and accelerated prion disease after NG2 glia depletion. We examined neuronal survival upon inhibition of Ptges activity by C118 and C934 in normal and prion-infected COCS with or without

NG2 glia depletion. Consistent with the above findings (**Fig. 2A-B**), loss of NG2 glia strongly enhanced prion-induced neurodegeneration (**Fig. 5A-B**). However, this enhancement was largely blocked by C118 and C934 treatment (**Fig. 5A-B**). This suggests that the enhanced neurodegeneration in NG2 glia depleted COCS is mediated by PGE2.

We then crossed Pdgfrα-CreER mice and iDTR mice with Cox2Luc mice to generate Pdgfrα^{iDTR}/Cox2Luc mice. Pdgfrα-CreER/Cox2Luc and iDTR/Cox2Luc mice served as controls (Ctrl/Cox2Luc). We infected Pdgfrα^{iDTR}/Cox2Luc and Ctrl/Cox2Luc mice with prions and compared them to prion inoculated Pdgfrα^{iDTR} and genetically matched control mice (designated as Pdgfrα^{iDTR}/WT and Ctrl/WT mice, respectively). All mice were treated with tamoxifen one month before prion inoculation and injected with DT at 16 wpi. As expected, loss of NG2 glia

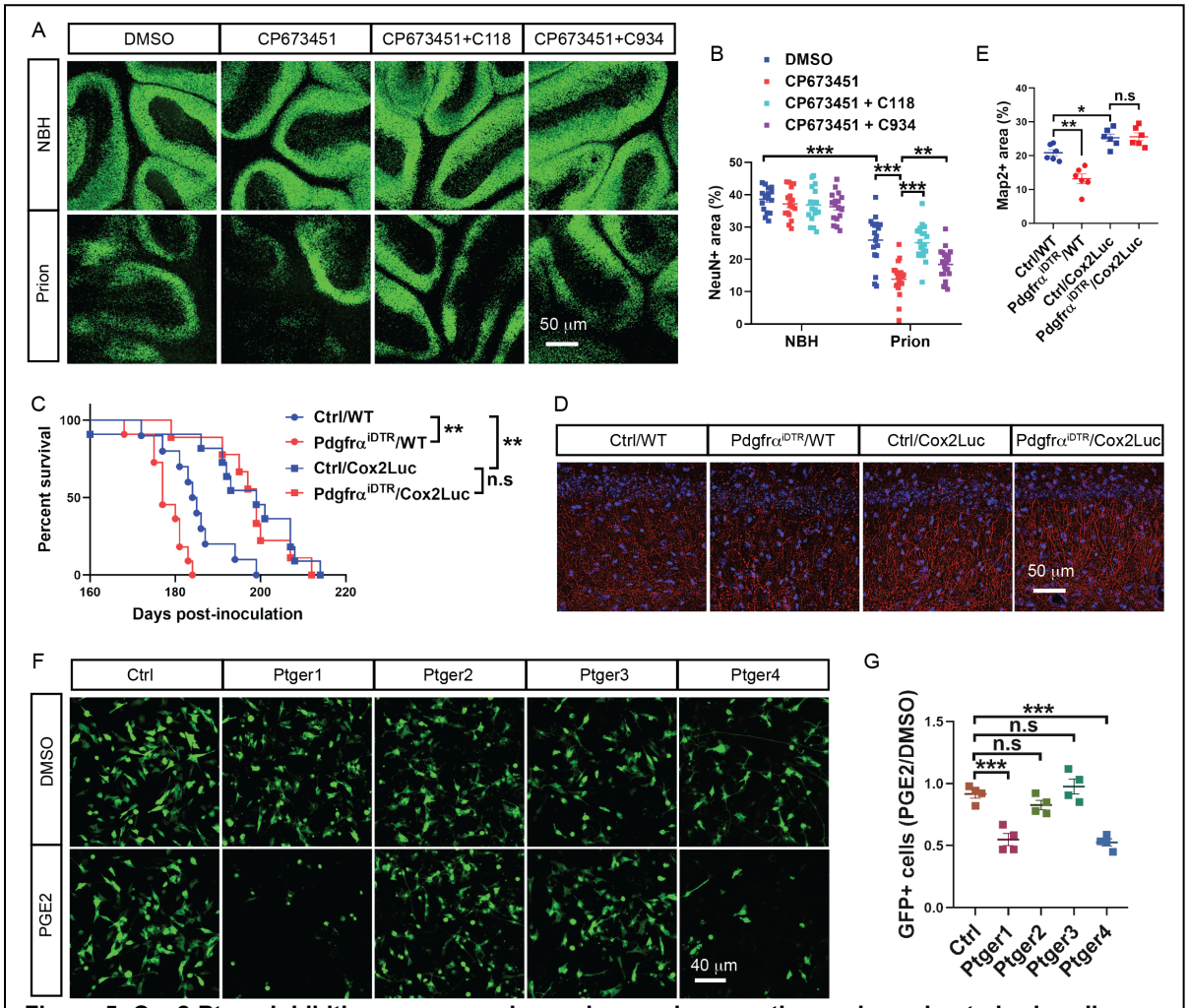

Figure 5, Cox2-Ptges inhibition rescues enhanced neurodegeneration and accelerated prion disease development after NG2 glia depletion. **A-B**, NeuN immunofluorescence (A) and quantification (B) showing that the enhanced neurodegeneration in prion-infected, NG2 glia-depleted (CP673451) COCS can be rescued by treatment with Ptges inhibitors C118 and C934. n = 16 slices/condition. **C**, Cox2 ablation (Cox2Luc) suppresses the acceleration of prion disease in NG2 glia-depleted (Pdgfrα^{iDTR}) mice. NG2 glia depletion was induced at 16 wpi. **D-E**, Map2 immunofluorescence (D) and quantification (E) showing enhanced dendritic pathology in NG2 glia-depleted (Pdgfrα^{iDTR}) hippocampi of prion-infected mice, and its rescue by Cox2 ablation (Cox2Luc). n = 6 mice/group. **F-G**, Live-cell images (F) and quantitative analysis (G) of chronically prion infected HovS cells expressing control (Ctrl) transgene or one of the four PGE2 receptors (Ptger). Effects of PGE2 treatment on prion-induced cell toxicity were measured with the ratio of GFP signals under the PGE2 condition against the DMSO condition. n = 4 independent experiments; 4 technical repeats/experiment.

significantly accelerated prion disease in Pdgfrα^{iDTR}/WT mice compared to Ctrl/WT mice (**Fig. 5C**), consistent with the abovementioned findings (**Fig. 2C**). However, the accelerated prion disease in NG2 glia-depleted mice was almost completely rescued in Pdgfrα^{iDTR}/Cox2Luc mice compared to Ctrl/Cox2Luc mice (**Fig. 5C**), and both Pdgfrα^{iDTR}/Cox2Luc mice and Ctrl/Cox2Luc mice survived drastically longer than Pdgfrα^{iDTR}/WT and Ctrl/WT mice (**Fig. 5C**). Loss of Cox2 also rescued the enhanced prion-induced dendritic pathology in Pdgfrα^{iDTR}/Cox2Luc mice compared to Pdgfrα^{iDTR}/WT mice (**Fig. 5D-E**). These findings confirm that increased PGE2 biosynthesis underlies the enhanced prion neurotoxicity and accelerated prion disease in NG2 glia deficient mice.

PGE2 enhances prion neurotoxicity through the EP1 and EP4 receptors

To investigate how PGE2 promotes prion-induced neurodegeneration, we first examined the cellular localization of its receptors, including prostaglandin E receptor 1 (Ptger1, also known as EP1), Ptger2 (also known as EP2), Ptger3 (also known as EP3) and Ptger4 (also known as EP4), in the adult mouse brain by immunofluorescence. We found that all four PGE2 receptors were expressed by neurons (**Supplementary fig. 7**). To determine which receptor might be responsible for the enhanced prion neurotoxicity, we expressed them one by one together with GFP in HovS cells chronically infected with prions (Avar, Heinzer et al. 2020) through lentiviral transduction, and examined death of HovS cells in the presence or absence of PGE2. We found that the number of GFP+ HovS cells were comparable between PGE2 and DMSO treated groups when Ptger2, Ptger3 or a control construct was expressed (**Fig. 5F-G**). However, expression of Ptger1 and Ptger4 reduced the survival of HovS cells in PGE2 treated groups compared to DMSO treated controls (**Fig. 5F-G**). Furthermore, we observed an abnormal morphology of surviving HovS cells, characterized by retraction of cellular processes and shrinkage of cell bodies, after PGE2 treatment only when Ptger1 and Ptger4 were expressed (**Fig. 5F**). Therefore, PGE2 enhances prion-induced neurodegeneration mainly through activating the Ptger1 and Ptger4 mediated signaling in neurons.

Discussion

Oligodendrocyte lineage cells have long been considered as supportive components of the CNS and bystanders in neurogenerative diseases (Ettle, Schlachetzki et al. 2016). However, accumulating evidence suggest that this cell lineage may have additional functions other than producing myelin sheath (Funfschilling, Supplie et al. 2012, Liu and Zhou 2013, Fruhbeis, Kuo-Elsner et al. 2020), and may be actively involved in neurodegenerative processes (Lee, Morrison et al. 2012, Pandey, Shen et al. 2022). Here we found that loss of oligodendrocyte precursor cells unleashed a microglial pathway responsible for PGE2 biosynthesis, which enhances prion induced neurotoxicity and accelerates prion disease in animal models (**Supplementary fig. 8**). These data place oligodendrocyte precursor cells at the center stage of a non-cell-autonomous interaction network during prion infection, and support a protective role of these cells during chronic neurodegeneration.

The study of the functions of oligodendrocyte-lineage cells was limited by the lack of efficient and specific ways to manipulate them ex vivo and in vivo. To overcome this difficulty, we previously established experimental approaches to deplete oligodendrocyte precursor cells in cultured brain slices and in adult mouse brains (Liu and Aguzzi 2020), which formed the basis for the discoveries described here. Adaption of these tools to further models of neurodegeneration, such as AD and PD, would facilitate the investigations of disease-specific roles of oligodendrocyte precursor cells.

We found that depletion of oligodendrocyte precursor cells augmented the PGE2 biosynthesis pathway in cultured brain slices and adult mouse brains after prion infection, revealing a previously unknown regulatory mechanism of PGE2 signaling in the CNS. The role of PGE2 signaling in prion disease and prion-induced neurodegeneration was undefined, but PGE2 levels were found to be increased in the CSF of prion disease patients and correlated with the speed of disease progression (Minghetti, Greco et al. 2000, Minghetti, Cardone et al. 2002). Our findings indicate that PGE2 signaling is a strong enhancer of prion neurotoxicity and a potent driver of prion disease development, which underlies the enhanced neurodegeneration and accelerated prion disease in mice deficient of oligodendrocyte precursor cells. Furthermore, we found that PGE2 enhanced prion-induced neurodegeneration possibly through directly binding to its receptors, such as EP1 and EP4, on neuronal cells. These data suggest that Ptges inhibitors blocking PGE2 biosynthesis, such as C118 and C934 (Larsson, Steinmetz et al. 2019), which were tested in the current study, as well as EP1 and EP4 signaling antagonists, may represent good drug candidates for the treatment of prion disease.

We previously reported that oligodendrocyte precursor cells are required for maintaining the homeostatic state of microglia; however, loss of them did not result in microglia activation and neuroinflammation under normal conditions (Liu and Aguzzi 2020). Here, we found that this is true even in the context of prion infections, suggesting that loss of microglial homeostatic state

does not necessarily result in enhanced neuroinflammatory responses. Nevertheless, we found that deficiency of oligodendrocyte precursor cells dysregulates the PGE2 biosynthesis pathway in microglia. It is unclear whether dysregulation of the PGE2 biosynthesis is the cause or consequence of switching microglial cellular states in the absence of oligodendrocyte precursor cells. Furthermore, the molecular mechanisms underlying how oligodendrocyte precursor cells control the microglial PGE2 biosynthesis pathway is unknown. Finally, future studies might focus on extending the current findings to other neurodegenerative disorders and developing approaches that promote the beneficial activities of oligodendrocyte precursor cells, which may hold enormous potential for novel disease-modifying therapies.

Materials and methods

Mouse experiments

C57BL6/J mice were obtained from Charles River, Germany. Tga20 mice (Fischer, Rulicke et al. 1996) were obtained from Laboratory Animal Services Center at University of Zurich, Switzerland. Pdgfrα-CreER mice (Stock No: 018280), iDTR mice (Stock No: 007900) and Cox2Luc mice (Stock No: 030853) were obtained from the Jackson Laboratory, USA. Double transgenic Pdgfrα-CreER/iDTR (Pdgfrα^{iDTR}) mice were generated by crossing the Pdgfrα-CreER mice with the iDTR mice. To induce Cre activity and DTR expression in NG2 glia, Pdgfrα^{iDTR} mice were fed with tamoxifen-containing diet (ENVIGO, TD. 55125.I) for 4 weeks as reported previously (Liu and Aguzzi 2020). To generate Pdgfrα^{iDTR} mice on a Cox2Luc background, Pdgfrα-CreER mice and iDTR mice were first crossed with the Cox2Luc mice, then the resulting Pdgfrα-CreER mice and iDTR mice on the Cox2Luc background were crossed with each other. Littermates of the experimental groups were used as controls. All animal experiments in the current study were performed according to swiss federal guidelines and had been approved by the Animal Experimentation Committee of the Canton of Zurich under the permits 040/2015, 139/2016, 243/2018 and 236/2019.

Prion inoculation

Intracerebral prion inoculation was performed as previously described (Liu, Senatore et al. 2022). Briefly, adult mice were anesthetized with isoflurane and injected in the right hemisphere of the brain with 30 μl 0.01% w/v brain homogenates derived from adult C57BL6/J mice suffering from terminal prion disease. Prion strain used in the current study was the Rocky Mountain Laboratory strain of scrapie, passage 6. Mice inoculated with 30 μl 0.01% w/v non-infectious brain homogenates were used as controls. After prion inoculation, the health status of mice was closely monitored, and body weights of mice were recorded once per week. For experiments evaluating survival time after prion inoculation, mice were euthanized when they showed terminal disease symptoms or reached more than 20% loss of body weight. For biochemical and immunohistochemical analysis, mice were euthanized at specific time points after prion inoculation for tissue collection. To avoid potential influences of tamoxifen on prion disease development, mouse strains (e.g., Pdgfrα-CreER, iDTR and Pdgfrα^{iDTR} mice on WT or Cox2Luc background) went through tamoxifen food treatment was inoculated at least 4 weeks after switching back to the normal diet.

Cerebellar organotypic cultured slices (COCS)

COCS were prepared according to a previously published protocol (Falsig and Aguzzi 2008). Briefly, cerebella from 12-day old C57BL/6J or Tga20 pups were dissected, embedded in low

melting point agarose (Invitrogen, 15517-022) and cut into 350-μm thick slices with vibratome (Leica, VT1000S) in cold Gey's balanced salt solution (GBSS) supplemented with the glutamate receptor antagonist kynurenic acid (1 mM, Sigma, K3375) and glucose (33.33 mM, Sigma, G8769). Slices with intact morphology were collected into GBSS supplemented with kynurenic acid and glucose (GBSSK) and washed briefly for 3 times. Afterwards, brain slices were exposed to either 0.01% w/v prion-containing brain homogenates or 0.01% w/v brain homogenates derived from healthy mice for 1 hour at 4 °C and washed for 5 times in GBSSK. Six to eight slices were put on a Millicell-CM Biopore PTFE membrane insert (Millipore, PICM 03050) and kept on slice culture medium containing 50% MEM, 25% BME, 25% inactivated horse serum, 0.65% w/v glucose (MERCK, G8769), 1% GlutaMax (ThermoFisher Scientific, 35050061) and 1% penicillin/streptomycin (ThermoFisher Scientific, 10378016) at 37 °C in a tissue culture incubator. Slice culture medium was changed 3 times per week.

Treatment of brain slice cultures

Prostaglandin E2 (PGE2, sc-201225) and prostaglandin D2 (PGD2, sc-201221) were purchased from Santa Cruz Biotechnology. Prostaglandin E synthase (Ptges) inhibitors C118 and C934 (Larsson, Steinmetz et al. 2019) were obtained from Dr. Per-Johan Jakobsson at Karolinska Institutet, Sweden. All the above compounds were dissolved in DMSO (Sigma, 472301) and stored at −80 °C in aliquots. Treatments of COCS with PGE2 (1 μM), PGD2 (1 μM), C118 (2 μM) and C934 (2 μM) were started from 14 days after the cultures were established and lasted for 35 days. COCS treated with same amounts of DMSO were used as controls. Recombinant human PDGFAA (110-13A) was purchased from Peprotech, dissolved in Opti-MEM and stored at -20 °C in aliquots. Treatment of COCS with PDGFAA (40 ng/ml) was performed following the same protocol as with the compounds, except that COCS treated with Opti-MEM were used as controls.

NG2 glia depletion

NG2 glia depletion in COCS and in vivo was performed as previously described (Liu and Aguzzi 2020). Briefly, to achieve ex vivo NG2 glia depletion, CP673451 (MedChemExpress, HY-12050) was supplemented in slice culture medium with the concentration of 1 μM. Treatments were started from 14 days after the cultures were established and lasted for 35 days (for long-term continuous depletion) or 9 days (for short-term transient depletion). Fresh CP673451 were added every time when the culture medium was changed. COCS treated with same amount of DMSO were used as controls. To achieve in vivo NG2 glia depletion, tamoxifen-treated Pdgfrα^{iDTR} mice were injected intraperitoneally with diphtheria toxin (DT, Sigma, D0564) diluted in saline for five consecutive days (two injections per day with an 8-hour

interval, 200 ng per injection). DT-injected tamoxifen-treated Pdgfrα-CreER mice and iDTR mice from same litters of the Pdgfrα^{iDTR} mice were pooled together and used as controls.

Lentiviral production

Lenti-vectors used for expressing human PGE2 receptors EP1 (pLenti-PTGER1-mGFP-P2A-Puro, RC208597L4), EP2 (pLenti-PTGER2-mGFP-P2A-Puro, RC210883L4), EP3 (pLenti-PTGER3-mGFP-P2A-Puro, RC220173L4) and EP4 (pLenti-PTGER4-mGFP-P2A-Puro, RC210932L4) were purchased from OriGene Technologies. A control vector (pLenti-HygR-mGFP-P2A-Puro) was produced in house by replacing the EP2 sequence in the pLenti-PTGER2-mGFP-P2A-Puro plasmid with the sequence of the Hygromycin resistant gene (HygR). All plasmids were verified by Sanger sequencing before lentiviral production in HEK293T cells maintained in Opti-MEM supplemented with 10% fetal bovine serum (FBS). Briefly, HEK293T cells were seeded in 10-cm cell culture dishes and transfected at ~ 80% confluency with a packaging plasmid mixture (transgene plasmid; VSVG plasmid; PAX2 plasmid) using FuGENE HD transfection reagent (Promega, E2311). Twenty-four hours after transfection, culture medium was changed to remove the transfection reagent. After another 48 hours, the culture medium containing lentivirus was collected, centrifuged at 1500g for 10 min and filtered through 0.45-micron Whatman filter units (GE Healthcare, 10462100). High-titer lentivirus was produced by concentrating the filtered supernatant with Lenti-X concentrator (Takara, 631231) and stored at -80 °C in aliquots.

In vitro prion toxicity

HovS cells (Avar, Heinzer et al. 2020), a subclone of the human SH-SY5Y cell line, where the human PRNP gene was replaced with the ovine PRNP VRQ allele, were maintained in Opti-MEM medium supplemented with 10% FBS, 1% MEM Non-Essential Amino Acids (MEM-NEAA; ThermoFisher Scientific, 11140050), 1% GlutaMax (ThermoFisher Scientific, 35050061), 1% penicillin/streptomycin (ThermoFisher Scientific, 10378016) and 400 mg/ml Geneticin (ThermoFisher Scientifc, 10131027). To establish a cellular model of chronic prion-infection, HovS cells were exposed to brain homogenates derived from PG127 prion-infected tg338 mice and passaged for at least 10 times before being used for experiments. To investigate the effects of PGE2 and the involved PGE2 receptors in prion-induced toxicity, PG127 HovS cells were seeded into 96-well plates. Twenty-four hours after seeding, cells were transduced with either control lentivirus or lentivirus harboring one of the four EP receptor transgenes. After 48 hours, the lentivirus-containing culture medium was removed, and fresh culture medium supplemented with DMSO or PGE2 (10 μM) was added in the wells (4 technical repeats for each condition) and incubated for another 48 hours. Finally, GFP positive

cells (cells infected with lentivirus) were imaged with a Nikon Eclipse Ti2-E confocal fluorescent microscope and quantified with ImageJ.

Western blotting

Western blotting was performed as previously described (Liu, Sorce et al. 2018). Briefly, cultured brain slices or collected brain tissues were lysed with a bead mill homogenizer in RIPA buffer supplemented with proteinase inhibitor cocktail cOmplete (MERCK, 11697498001) and Phosphatase inhibitor cocktail PhosSTOP (MERCK, 4906845001). After centrifuge, protein concentrations in the supernatant were quantified with the BCA method. Protein samples were then mixed with western blotting loading buffer and boiled for 5 minutes at 95 °C before being loaded onto the gels. For western blotting aimed to detect prions, samples were first digested with 10 μg/ml (for COCS) or 20 μg/ml (for brain tissues) proteinase K for 30 minutes at 37 °C, then mixed with western blotting loading buffer and boiled for 5 minutes at 95 °C. The following primary antibodies were used: mouse monoclonal antibody against actin (1:10,000, Merck Millipore, MAB1501R); mouse monoclonal antibody against PrP (POM1, 1:5000, homemade); rabbit polyclonal antibody against NG2 (1:500, MERCK, AB5320) and PDGFRα (1:500, Santa Cruz, SC-338); rabbit monoclonal antibody against NeuN (1:2000, Abcam, ab177487). Depending on the primary antibodies used, suitable HRP-conjugated secondary antibodies (1:10,000, Jackson ImmunoResearch Laboratories) were chosen. Membranes were developed with Crescendo Western HRP Substrate (MERCK, WBLUR0500), visualized and digitized with ImageQuant (LAS-4000; Fujifilm, Japan). Optical densities of bands were analyzed using ImageJ.

Immunofluorescence

Immunofluorescent staining of cultured brain slices and cryosections was performed according to procedures published previously (Liu and Aguzzi 2020). For cultured brain slices: after removing culture medium, brain slices were washed with phosphate buffered saline (PBS) and fixed in 4% PFA for 30 min at room temperature. After several washes to remove residual PFA, brain slices were then permeabilized with PBST (PBS + 0.1% Triton X-100) for 2 hours at room temperature and blocked with 5% goat serum (GS) overnight at 4 °C before adding primary antibodies. For cryosections: mice were perfused transcardially with 20 ml PBS and 20 ml 4% PFA. The dissected brains were then postfixed with 4% PFA for 4 hr or overnight in the fridge. After removing PFA and brief wash with PBS, brains were transferred into 30% sucrose solution for dehydration, and kept at 4°C. After dehydration was complete, brains were cut into 25-μm thick cryosections. To perform immunostaining, cryosetions were permeablized in PBST for 2 hours and blocked with 5% GS for 2 hours before incubation in primary antibodies. The following primary antibodies were used: rabbit polyclonal antibody

against NG2 (1:500, a gift from Prof. Stallcup), rabbit monoclonal antibody against NeuN (1:1000, Abcam, ab177487), rabbit polyclonal antibody against Iba1 (1:500, Wako, 019-19741), Rat monoclonal antibody against Cd68 (1:200, BioRad, MCA1957), rabbit polyclonal antibody against Map2 (1:200, Biolegend, 840601), rabbit polyclonal antibody against EP1 (1:200, Bioss Antibodies, BS-6316R), rabbit monoclonal antibody against EP2 (1:200, Abcam, ab167171), rabbit polyclonal antibody against EP3 (1:200, Cayman Chemical, 101760) and mouse monoclonal antibody against EP4 (1:200, ProteinTech, 66921-1-Ig). Cultured brain slices were incubated in the primary antibody at 4°C for 3 days, and cryosections were incubated in the primary antibody at 4°C overnight. After several washes in PBST, cultured brain slices were incubated in suitable secondary antibodies overnight at 4°C and cryosections were incubated in suitable secondary antibodies for 2 hours at room temperature. Immunofluorescent images were captured using the FLUOVIEW FV10i confocal microscope (Olympus Life Science), and were quantified using ImageJ.

Quantitative real-time PCR

To perform quantitative real-time-PCR (qRT-PCR) analysis, total RNA from cultured brain slices or collected brain tissues was extracted using TRIzol reagent (ThermoFisher Scientific, 15596026). QuantiTect Reverse Transcription kit (QIAGEN, 205311) was used to synthesize cDNA from the extracted RNA samples. qRT-PCR was performed on a ViiA7 Real-Time PCR system (Applied Biosystems, USA) using the SYBR Green PCR Master Mix (ThermalFisher Scientifc, 4309155). We used the following primers for qRT-PCR analysis: Mouse actin: sense, 5′-AGATCAAGATCATTGCTCCTCCT-3′, antisense, 5′-ACGCAGCTCAGTAACAGTCC-3′. Mouse NG2: sense, 5′-ACCCAGGCTGAGGTAAATGC-3′, antisense, 5′-ACAGGCAGCATCGAAAGACA-3′. Mouse Pdgfrα: sense, 5′-ATTAAGCCGGTCCCAACCTG-3′, antisense, 5′-AATGGGACCTGACTTGGTGC-3′. Mouse TNFα: sense, 5′-ACGTCGTAGCAAACCACCAA-3′, antisense, 5′-ATAGCAAATCGGCTGACGGT-3′. Mouse IL1β: sense, 5′-TGCAGCTGGAGAGTGTGGATCCC-3′, antisense, 5′-TGTGCTCTGCTTGTGAGGTGCTG-3′. Mouse IL12β: sense, 5′-TGGTTTGCCATCGTTTTGCTG-3′, antisense, 5′-ACAGGTGAGGTTCACTGTTTCT-3′. Mouse Cox1: sense, 5′-TCCATCCACTCCCAGAGTCAT-3′, antisense, 5′-ACAACAGGGATTGACTGGTGA-3′. Mouse Cox2: sense, 5′-GGGCCATGGAGTGGACTTAAA-3′, antisense, 5′-ACTCTGTTGTGCTCCCGAAG-3′. Mouse Ptges: sense, 5′-TCTCACTCTCAGTCCCGGTG-3′, antisense, 5′-GGGGTTGGCAAAAGCCTTC-3′. Mouse Ptgds: sense, 5′-GCTCCTTCTGCCCAGTTTTCC-3′, antisense, 5′-CCCCAGGAACTTGTCTTGTTGA-3′.

2.10 Statistical analyses

Unless otherwise mentioned, unpaired, two-tailed student's t test was used for comparing data from two groups. All data were presented as mean ± SEM. To compare the incubation time of prion-inoculated mice, survival curves were estimated using the Kaplan-Meier method and compared statistically using the log rank test. Statistical analysis and data visualization were done using GraphPad Prism 9. P-value < 0.05 was considered statistically significant.

Acknowledgements

We thank Dr. William Stallcup for providing the polyclonal antibodies against NG2, Julie Domange, Mirzet Delic, Maria Svercelova and Marija Mihailova for excellent assistance. YL was supported by a Forschungskredit PostDoc grant (FK Liu 19-042). AA was supported by an Advanced Grant of the European Research Council (ERC 670958), the Swiss National Foundation (SNF 179040), and the Nomis Foundation.

Author Contributions

YL and AA conceptualized the study; YL designed and performed the experiments with help from JG, MM and MK. PJ provided the Ptges inhibitors and helpful guidance on relevant experiments. YL and AA wrote the manuscript.

Declaration of Interests

The authors declare no competing interest.

Reference

Aguzzi, A. and Y. Liu (2017). "A role for astroglia in prion diseases." J Exp Med **214**(12): 3477-3479.

Akhtar, S., A. Wenborn, S. Brandner, J. Collinge and S. E. Lloyd (2011). "Sex effects in mouse prion disease incubation time." PLoS One **6**(12): e28741.

Alonso, G. (2005). "NG2 proteoglycan-expressing cells of the adult rat brain: possible involvement in the formation of glial scar astrocytes following stab wound." Glia **49**(3): 318-338.

Avar, M., D. Heinzer, N. Steinke, B. Dogancay, R. Moos, S. Lugan, C. Cosenza, S. Hornemann, O. Andreoletti and A. Aguzzi (2020). "Prion infection, transmission, and cytopathology modeled in a low-biohazard human cell line." Life Sci Alliance **3**(8).

Brandner, S., S. Isenmann, A. Raeber, M. Fischer, A. Sailer, Y. Kobayashi, S. Marino, C. Weissmann and A. Aguzzi (1996). "Normal host prion protein necessary for scrapie-induced neurotoxicity." Nature **379**(6563): 339-343.

Bueler, H., A. Aguzzi, A. Sailer, R. A. Greiner, P. Autenried, M. Aguet and C. Weissmann (1993). "Mice devoid of PrP are resistant to scrapie." Cell **73**(7): 1339-1347.

Calver, A. R., A. C. Hall, W. P. Yu, F. S. Walsh, J. K. Heath, C. Betsholtz and W. D. Richardson (1998). "Oligodendrocyte population dynamics and the role of PDGF in vivo." Neuron **20**(5): 869-882.

Chen, W. T., A. Lu, K. Craessaerts, B. Pavie, C. Sala Frigerio, N. Corthout, X. Qian, J. Lalakova, M. Kuhnemund, I. Voytyuk, L. Wolfs, R. Mancuso, E. Salta, S. Balusu, A. Snellinx, S. Munck, A. Jurek, J. Fernandez Navarro, T. C. Saido, I. Huitinga, J. Lundeberg, M. Fiers and B. De Strooper (2020). "Spatial Transcriptomics and In Situ Sequencing to Study Alzheimer's Disease." Cell **182**(4): 976-991 e919.

Dimitriadis, A., F. Zhang, T. Murphy, T. Trainer, Z. Jaunmuktane, C. Schmidt, T. Nazari, J. Linehan, S. Brandner, J. Collinge, S. Mead and E. Viré (2022). "Single-nuclei transcriptomics of mammalian prion diseases identifies dynamic gene signatures shared between species." bioRxiv: 2022.2009.2013.507650.

Ettle, B., J. C. M. Schlachetzki and J. Winkler (2016). "Oligodendroglia and Myelin in Neurodegenerative Diseases: More Than Just Bystanders?" Mol Neurobiol **53**(5): 3046-3062.

Falsig, J. and A. Aguzzi (2008). "The prion organotypic slice culture assay--POSCA." Nat Protoc **3**(4): 555-562.

Fischer, M., T. Rulicke, A. Raeber, A. Sailer, M. Moser, B. Oesch, S. Brandner, A. Aguzzi and C. Weissmann (1996). "Prion protein (PrP) with amino-proximal deletions restoring susceptibility of PrP knockout mice to scrapie." EMBO J **15**(6): 1255-1264.

Fruhbeis, C., W. P. Kuo-Elsner, C. Muller, K. Barth, L. Peris, S. Tenzer, W. Mobius, H. B. Werner, K. A. Nave, D. Frohlich and E. M. Kramer-Albers (2020). "Oligodendrocytes support axonal transport and maintenance via exosome secretion." PLoS Biol **18**(12): e3000621.

Fuhrmann, M., G. Mitteregger, H. Kretzschmar and J. Herms (2007). "Dendritic pathology in prion disease starts at the synaptic spine." J Neurosci **27**(23): 6224-6233.

Funfschilling, U., L. M. Supplie, D. Mahad, S. Boretius, A. S. Saab, J. Edgar, B. G. Brinkmann, C. M. Kassmann, I. D. Tzvetanova, W. Mobius, F. Diaz, D. Meijer, U. Suter, B. Hamprecht, M. W. Sereda, C. T. Moraes, J. Frahm, S. Goebbels and K. A. Nave (2012). "Glycolytic oligodendrocytes maintain myelin and long-term axonal integrity." Nature **485**(7399): 517-521.

Jin, X., T. R. Riew, H. L. Kim, J. H. Choi and M. Y. Lee (2018). "Morphological characterization of NG2 glia and their association with neuroglial cells in the 3-nitropropionic acid-lesioned striatum of rat." Sci Rep **8**(1): 5942.
Larsson, K., J. Steinmetz, F. Bergqvist, S. Arefin, L. Spahiu, J. Wannberg, S. C. Pawelzik, R. Morgenstern, P. Stenberg, K. Kublickiene, M. Korotkova and P. J. Jakobsson (2019). "Biological characterization of new inhibitors of microsomal PGE synthase-1 in preclinical models of inflammation and vascular tone." Br J Pharmacol **176**(24): 4625-4638.
Lee, Y., B. M. Morrison, Y. Li, S. Lengacher, M. H. Farah, P. N. Hoffman, Y. Liu, A. Tsingalia, L. Jin, P. W. Zhang, L. Pellerin, P. J. Magistretti and J. D. Rothstein (2012). "Oligodendroglia metabolically support axons and contribute to neurodegeneration." Nature **487**(7408): 443-448.
Liu, Y. and A. Aguzzi (2019). "Immunotherapy for neurodegeneration?" Science **364**(6436): 130-131.
Liu, Y. and A. Aguzzi (2020). "NG2 glia are required for maintaining microglia homeostatic state." Glia **68**(2): 345-355.
Liu, Y., A. Senatore, S. Sorce, M. Nuvolone, J. Guo, Z. H. Gumus and A. Aguzzi (2022). "Brain aging is faithfully modelled in organotypic brain slices and accelerated by prions." Commun Biol **5**(1): 557.
Liu, Y., S. Sorce, M. Nuvolone, J. Domange and A. Aguzzi (2018). "Lymphocyte activation gene 3 (Lag3) expression is increased in prion infections but does not modify disease progression." Sci Rep **8**(1): 14600.
Liu, Y. and J. Zhou (2013). "Oligodendrocytes in neurodegenerative diseases." Frontiers in Biology **8**(2): 127-133.
Loeuillet, C., P. Y. Boelle, C. Lemaire-Vieille, M. Baldazza, P. Naquet, P. Chambon, M. F. Cesbron-Delauw, A. J. Valleron, J. Gagnon and J. Y. Cesbron (2010). "Sex effect in mouse and human prion disease." J Infect Dis **202**(4): 648-654.
Mathys, H., J. Davila-Velderrain, Z. Peng, F. Gao, S. Mohammadi, J. Z. Young, M. Menon, L. He, F. Abdurrob, X. Jiang, A. J. Martorell, R. M. Ransohoff, B. P. Hafler, D. A. Bennett, M. Kellis and L. H. Tsai (2019). "Single-cell transcriptomic analysis of Alzheimer's disease." Nature **570**(7761): 332-337.
Minghetti, L., F. Cardone, A. Greco, M. Puopolo, G. Levi, A. J. Green, R. Knight and M. Pocchiari (2002). "Increased CSF levels of prostaglandin E(2) in variant Creutzfeldt-Jakob disease." Neurology **58**(1): 127-129.
Minghetti, L., A. Greco, F. Cardone, M. Puopolo, A. Ladogana, S. Almonti, C. Cunningham, V. H. Perry, M. Pocchiari and G. Levi (2000). "Increased brain synthesis of prostaglandin E2 and F2-isoprostane in human and experimental transmissible spongiform encephalopathies." J Neuropathol Exp Neurol **59**(10): 866-871.
Minikel, E. V., H. T. Zhao, J. Le, J. O'Moore, R. Pitstick, S. Graffam, G. A. Carlson, M. P. Kavanaugh, J. Kriz, J. B. Kim, J. Ma, H. Wille, J. Aiken, D. McKenzie, K. Doh-Ura, M. Beck, R. O'Keefe, J. Stathopoulos, T. Caron, S. L. Schreiber, J. B. Carroll, H. B. Kordasiewicz, D. E. Cabin and S. M. Vallabh (2020). "Prion protein lowering is a disease-modifying therapy across prion disease stages, strains and endpoints." Nucleic Acids Res **48**(19): 10615-10631.
Pandey, S., K. Shen, S. H. Lee, Y. A. Shen, Y. Wang, M. Otero-Garcia, N. Kotova, S. T. Vito, B. I. Laufer, D. F. Newton, M. G. Rezzonico, J. E. Hanson, J. S. Kaminker, C. J. Bohlen, T. J. Yuen and B. A. Friedman (2022). "Disease-associated oligodendrocyte responses across neurodegenerative diseases." Cell Rep **40**(8): 111189.

Slota, J. A., B. V. Sajesh, K. F. Frost, S. J. Medina and S. A. Booth (2022). "Dysregulation of neuroprotective astrocytes, a spectrum of microglial activation states, and altered hippocampal neurogenesis are revealed by single-cell RNA sequencing in prion disease." Acta Neuropathol Commun **10**(1): 161.
Sorce, S., M. Nuvolone, G. Russo, A. Chincisan, D. Heinzer, M. Avar, M. Pfammatter, P. Schwarz, M. Delic, M. Muller, S. Hornemann, D. Sanoudou, C. Scheckel and A. Aguzzi (2020). "Genome-wide transcriptomics identifies an early preclinical signature of prion infection." PLoS Pathog **16**(6): e1008653.
Wareham, L. K., S. A. Liddelow, S. Temple, L. I. Benowitz, A. Di Polo, C. Wellington, J. L. Goldberg, Z. He, X. Duan, G. Bu, A. A. Davis, K. Shekhar, A. Torre, D. C. Chan, M. V. Canto-Soler, J. G. Flanagan, P. Subramanian, S. Rossi, T. Brunner, D. E. Bovenkamp and D. J. Calkins (2022). "Solving neurodegeneration: common mechanisms and strategies for new treatments." Mol Neurodegener **17**(1): 23.

Supplementary figures

Supplementary figure 1, A-B, Experimental design of continuous (A) and transient (B) NG2 glia depletion in COCS. **C**, Representative NeuN and NG2 immunofluorescent images showing enhanced neurodegeneration in transiently NG2 glia-depleted (CP673451) COCS compared to NG2 glia intact (DMSO) COCS after prion infection. Nuclei were stained with DAPI (blue). **D**, Quantifications of NG2 immuno-intensity and NeuN positive area shown in C. n > 16 slices/condition. Here and in all following figures: *: $p < 0.05$; **: $p < 0.01$; ***: $p < 0.001$; n.s: not significant.

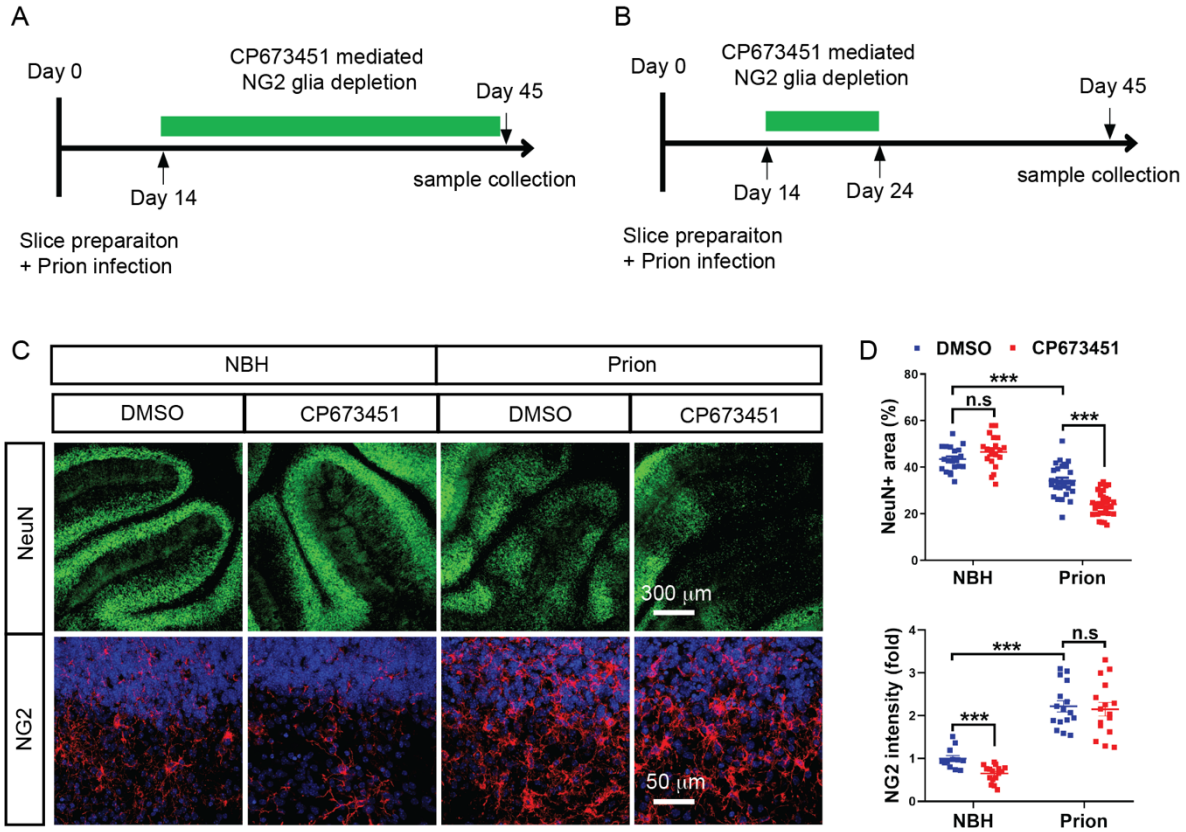

Supplementary figure 2, A, Experimental design of NG2 glia depletion in prion inoculated Pdgfrα^{iDTR} mice. Littermate Pdgfrα-CreER and iDTR mice were pooled together as control (Ctrl) and treated with tamoxifen and DT the same way as the Pdgfrα^{iDTR} mice. **B**, Survival curves showing accelerated prion disease in male but not female NG2 glia depleted (Pdgfrα^{iDTR}) mice compared to NG2 glia intact (Ctrl) mice after prion inoculation when NG2 glia depletion was induced at 12 wpi.

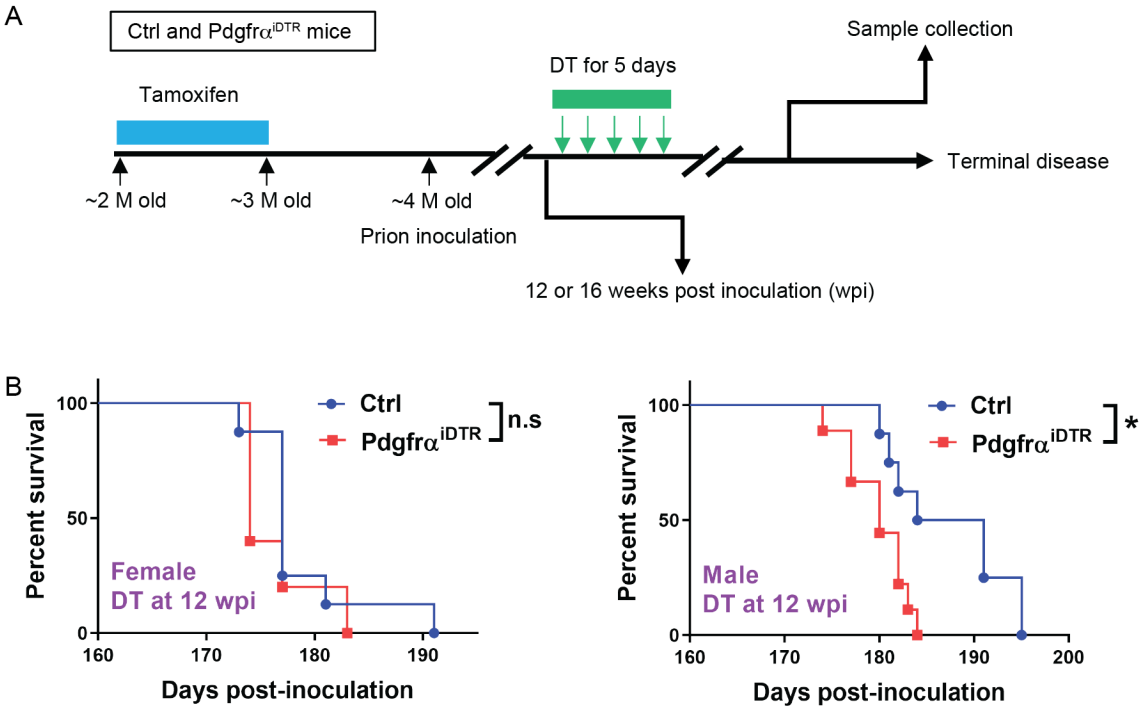

Supplementary figure 3, A-B, Western blots (A) and quantification (B) showing no changes of PrP^{C} in NG2 glia-depleted (CP673451) COCS compared to NG2 glia-intact (DMSO) COCS. n = 5 samples for DMSO and n = 4 samples for CP673451; 6 to 8 slices/sample. **C-D**, Western blots (C) and quantification (D) showing no changes of PK-resistant PrP^{Sc} in NG2 glia depleted (CP673451) COCS compared to NG2 glia intact (DMSO) COCS after prion infection. n = 5 samples for DMSO and n = 4 samples for CP673451; 6 to 8 slices/sample. **E-F**, Western blots (E) and quantification (F) showing no changes of PrP^{C} in the brains of NG2 glia depleted ($Pdgfr\alpha^{iDTR}$) mice compared to NG2 glia intact (Ctrl) mice. n = 4 mice for Ctrl and n = 5 mice for $Pdgfr\alpha^{iDTR}$. **G-H**, Western blots (G) and quantification (H) showing no changes of PK-resistant PrP^{Sc} in the brains of NG2 glia depleted ($Pdgfr\alpha^{iDTR}$) mice compared to NG2 glia intact (Ctrl) mice after prion infection. NG2 glia depletion was induced at 16 wpi. n = 4 mice for Ctrl and n = 5 mice for $Pdgfr\alpha^{iDTR}$.

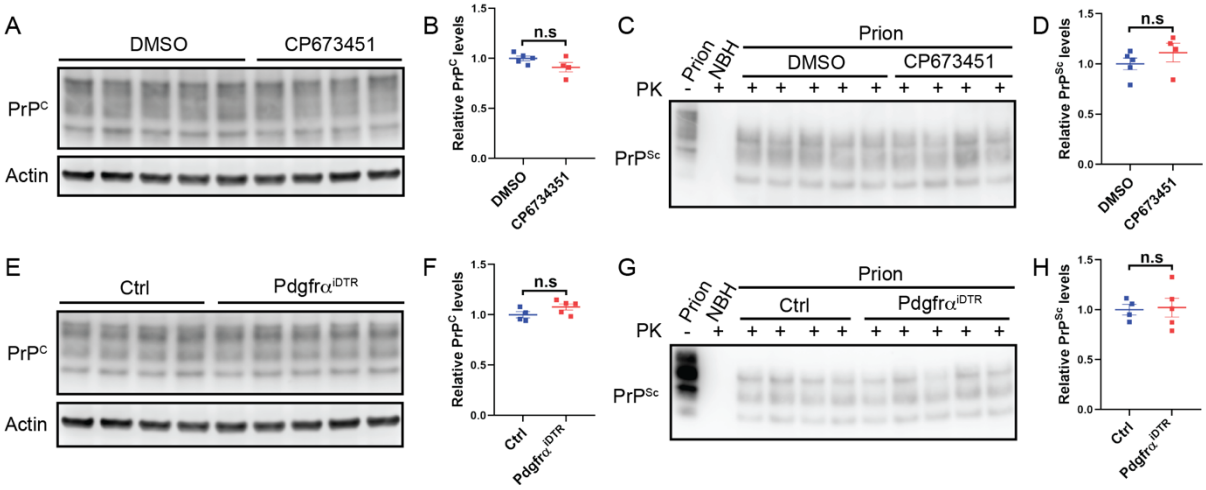

Supplementary figure 4, A-B, Cd68 immunofluorescence (A) and quantification (B) showing similar levels of microglia activation in NG2 glia depleted (CP673451) COCS compared to NG2 glia intact (DMSO) COCS after prion infection. Nuclei: DAPI (blue). n > 16 slices/condition. **C-D**, Iba1 and Cd68 immunofluorescence (C) and quantification (D) showing similar levels of microglia activation in the brains of NG2 glia depleted (Pdgfrα^{iDTR}) mice compared to NG2 glia intact (Ctrl) mice after prion infection. NG2 glia depletion was induced at 16 wpi. Nuclei: DAPI (blue). n = 6 mice/group.

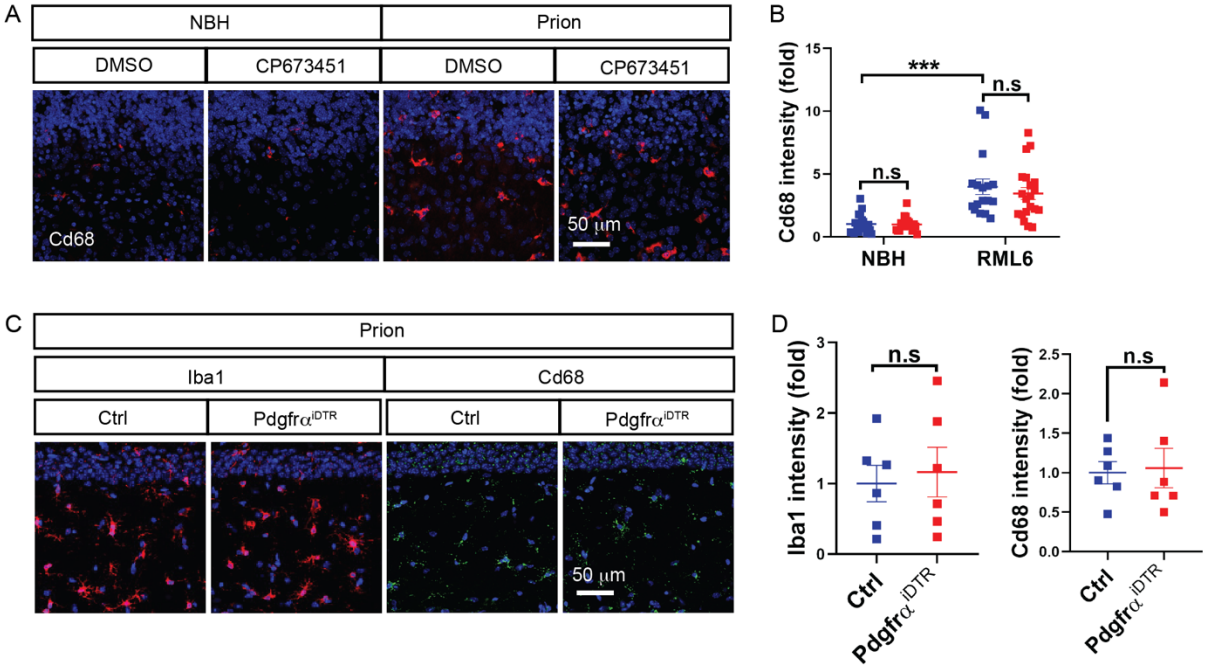

Supplementary figure 5, A, qRT-PCR results showing minimal changes of proinflammatory factors TNFα, IL1β and IL12β in NG2 glia depleted (CP673451) COCS compared to NG2 glia intact (DMSO) COCS after prion infection. n = 6 samples/condition; 6 to 8 slices/sample. **B**, qRT-PCR results showing no changes of proinflammatory factors TNFα, IL1β and IL12β in the brains of NG2 glia depleted (Pdgfrα^{iDTR}) mice compared to NG2 glia intact (Ctrl) mice after prion inoculation. n = 5 mice/group. NG2 glia depletion was induced at 16 wpi.

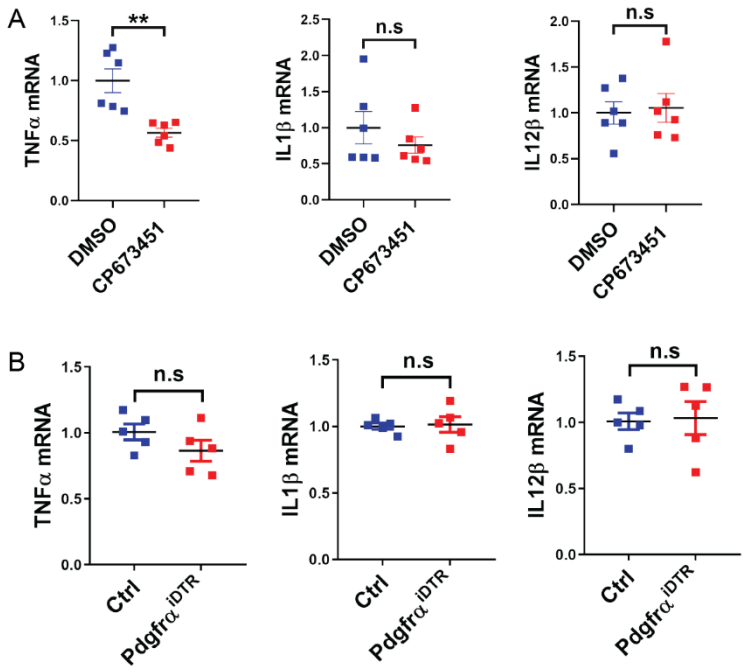

Supplementary figure 6, qRT-PCR results showing no changes of Cox1 and Ptgds in NG2 glia depleted (CP673451) COCS compared to NG2 glia intact (DMSO) COCS in the presence or absence of prions. n = 7 samples/condition; 6 to 8 slices/sample.

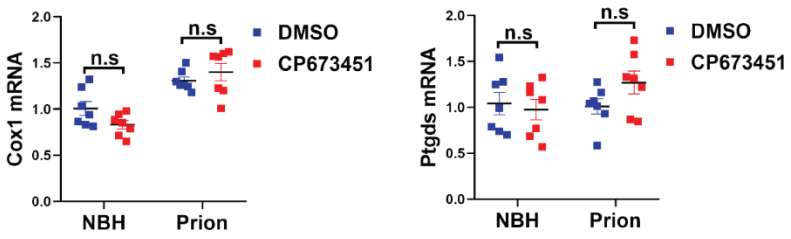

Supplementary figure 7, Immunofluorescence of NeuN and PGE2 receptors showing neuronal expression of Ptger1, Ptger2, Ptger3 and Ptger4 in the adult mouse brain. Scale bar: 50 μm.

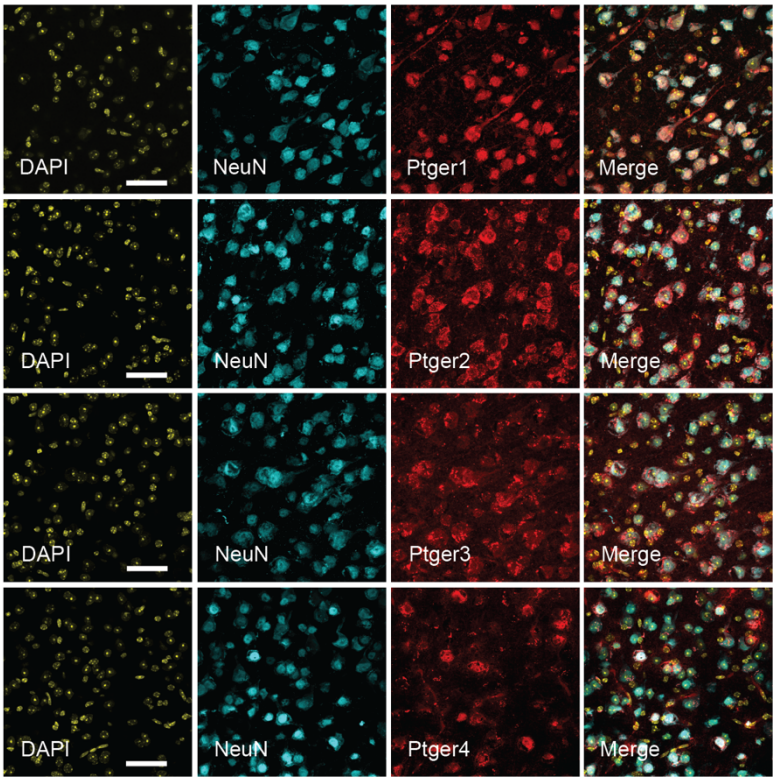

Supplementary figure 8, Diagram summarizing the main findings. In prion disease, microglia become activated due to prion replication, and upregulate the pathway responsible for PGE2 biosynthesis, which promotes prion-induced neurodegeneration through binding to neuronal EP1 and EP4 receptors. NG2 glia serve as a brake in this process, inhibiting microglial Cox2-Ptges pathway and PGE2 biosynthesis. The molecular mechanisms underlying how NG2 glia control microglial Cox2-Ptges pathway is not entirely understood.

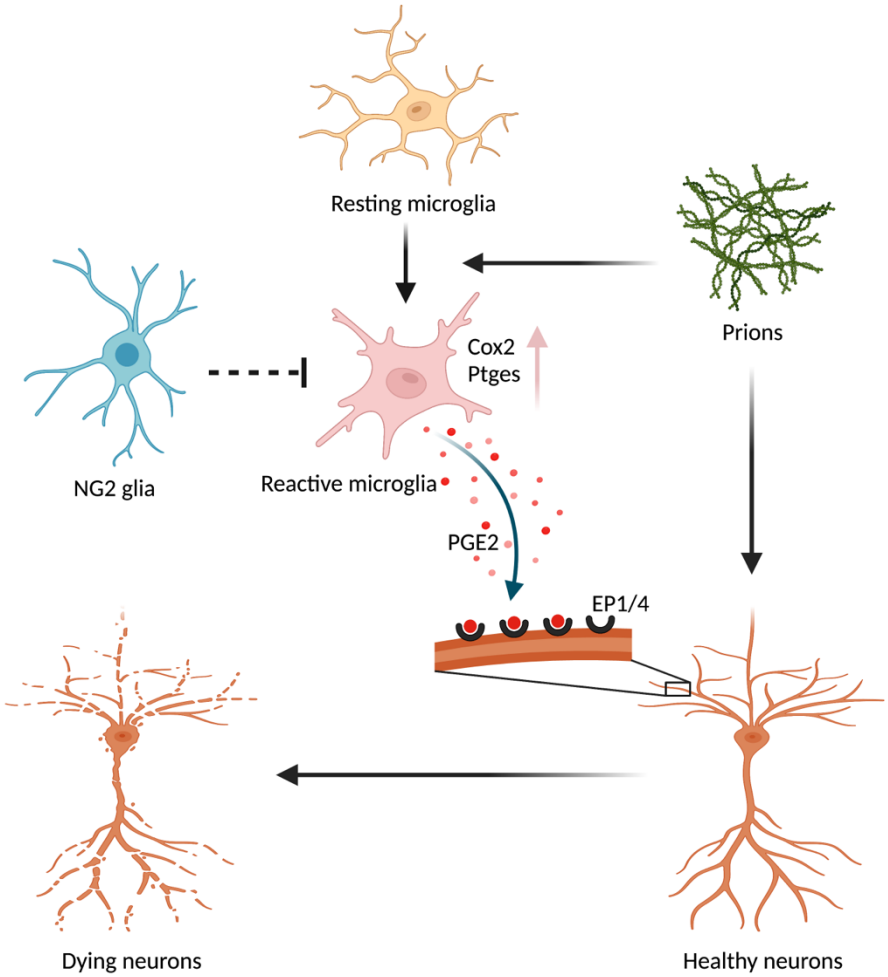
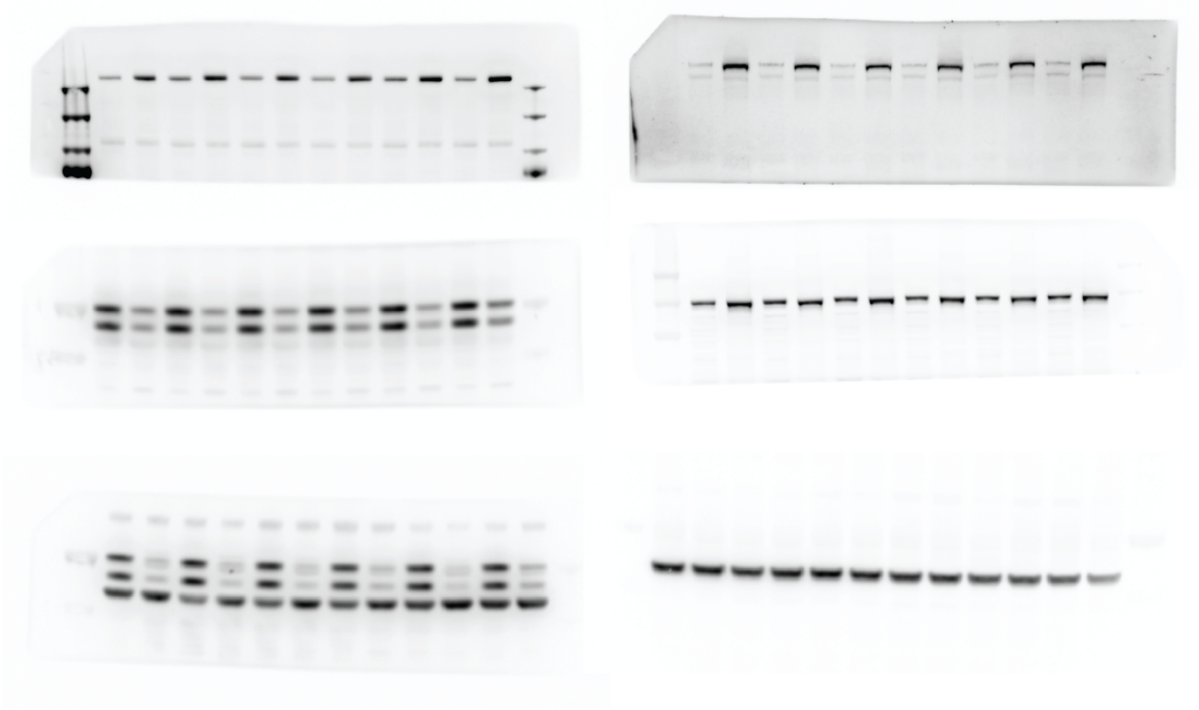
Supplementary figure 9, uncropped western blots shown in figure 1.